Available online at www.sciencedirect.com
SCIENCE DIRECT®
PERGAMON
International Journal of Heat and Mass Transfer 46 (2003) 2983–2992
International Journal of HEAT and MASS TRANSFER
www.elsevier.com/locate/ijhmt

# A fiber-optic Bragg grating sensor for simultaneous static and dynamic temperature measurement on a heated cylinder in cross-flow

Z.J. Wang [a], Y. Zhou [a,*], X.W. Wang [b], W. Jin [c]

[a] Department of Mechanical Engineering, The Hong Kong Polytechnic University, Hung Hom, Kowloon, Hong Kong
[b] Department of Mechanical Engineering, North China Institute of Astronautic Engineering, Langfang, Hebei, 065000 China
[c] Department of Electrical Engineering, The Hong Kong Polytechnic University, Hung Hom, Kowloon, Hong Kong

Received 17 June 2002; received in revised form 15 January 2003

**Abstract**

A fiber-optic Bragg grating (FBG) sensor is proposed to measure the local static temperature $\overline{\theta_s}$ and the fluctuating temperature $\theta_s$ on the surface of a heated circular cylinder subjected to a cross-flow. In order to validate the new technique, a type-$K$ thermocouple and a single hot wire are used to measure $\overline{\theta_s}$ and the near-wake streamwise fluctuating velocity $u$, respectively. The FBG sensor measurement of $\overline{\theta_s}$ agrees well with that simultaneously obtained by the thermocouple. The $\theta_s$-spectrum exhibits a prominent peak at the vortex shedding frequency, $f_s^* = f_s d/U_\infty \approx 0.2$ ($U_\infty$ is the free-stream velocity and $d$ is the cylinder diameter), consistent with the $u$-spectrum. In fact, the $\theta_s$ and $u$ signals are almost perfectly correlated at $f_s^*$. Furthermore, the measured $\overline{\theta_s}$ and root mean square value of $\theta_s$ are agreeable with previously reported Nusselt number data. These results demonstrate that the FBG sensor can be used to measure reliably both static and fluctuating temperatures. It is expected that the FBG sensor, because of its uniqueness in many aspects and being at an affordable cost, has an excellent prospect in temperature measurements.


## 1. Introduction

The study of the heat transfer characteristics of a heated circular cylinder in a cross-flow is of practical significance. As the Reynolds number, $Re$, exceeds a critical value, the boundary layer separates from the cylinder in a flip-flop manner. The separation point oscillates on the cylinder surface with an excursion of about 10° [1–3] and its mean location is dependent on $Re$ [4]. Naturally, the surface temperature fluctuates and the circumferential distribution of the static temperature is non-uniform. Local heat transfer from the cylinder to fluid varies azimuthally [5–7].

Experimental investigations of the heat transfer problem around a cylinder have been concentrated mainly on the measurement of the overall and local heat transfer coefficients, which were usually achieved by measuring the local heat flux and simultaneously the difference between local static surface temperature and bulk flow temperature [8,9]. Boulos and Pei [10] provided an excellent compendium of experimental and theoretical works on this topic. The data of the local fluctuating surface temperature is however scarce in spite of its significance in understanding the physics of heat transfer.

A number of well-established techniques are available for temperature measurements [11]. Morris [12] divided these techniques into eight categories based on their operating principle, i.e. thermal expansion method, thermocouples, resistive sensors, quartz thermometers, radiation thermometers, thermograph (thermal imaging), acoustic thermometers and fiber-optic temperature sensors. Most of these techniques are suitable either for a particular situation or for the measurement of the static temperature. For example, thermograph provides the static temperature distribution over a surface. Radiation

* Corresponding author. Tel.: +852-2766-6662.
*E-mail address:* mmyzhou@polyu.edu.hk (Y. Zhou).

0017-9310/03/$ - see front matter © 2003 Elsevier Science Ltd. All rights reserved.
doi:10.1016/S0017-9310(03)00070-X

thermometers are non-invasive, though largely suitable for a high temperature situation. Acoustic thermometers cater for needs to measure cryogenic temperature [12]. Fluctuating temperatures may be measured using thermocouples, resistive sensors [12–14]. Thermocouples suffer from a poor dynamic response and consequently are generally used to measure the static temperature or fluctuating temperature of a low frequency [11]. In the presence of a flow, this technique may be intrusive to the flow. Resistive sensors, such as fine wires used in the gas flow or thin metal films for solid surfaces, have good dynamic responses. However, this kind of sensors is usually associated with a bridge circuit, which may alter the temperature field under investigation [15]. Furthermore, both thermocouples and resistive sensors are prone to corruption by a neighbouring electromagnetic field.

The fiber-optic technique is relatively new for temperature sensors [12,14]. Gottlieb and Brandt [16] described the temperature-induced change of the refractive index of an optical fiber for measuring average temperature along its length. A typical application of fiber-optic temperature sensors is to monitor, or measure the average temperature or temperature distribution of large surfaces or long objects [14,17,18].

In the present study, it is proposed to use an alternative technique, the fiber-optic Bragg grating (FBG) sensor, to measure both static and fluctuating temperatures on the surface of a heated circular cylinder in a cross-flow. Hill et al. [19] first reported the formation of FBG within an optical fiber. An FBG is produced by varying the refractive index along an optical fiber. Since then, the FBG sensor has attracted considerable interest in various fields of engineering, including telecommunications, instrumentation and the measurements of strain, temperature and hydrostatic pressure [20]. The FBG sensor has many unique features. For example, its diameter could be as small as 80 μm. Therefore, its attachment to the structure would not seriously compromise the flow around the structure [21,22]. Its dynamic response is excellent. Furthermore, it is immune to corruption by neighbouring electromagnetic field and also causes no disturbance to the temperature field. In view of these advantages, the technique is most attractive for temperature measurements.

## 2. FBG sensor system

The FBG sensing system was built in-house [23]. It consists of a sensing FBG, a reference FBG, a broadband light source, a tunable optical filter (TOF), a fiber coupler, a photo-detector, a low pass electrical filter, a high pass electrical filter and the data acquisition and signal processing unit (Fig. 1). Light from the broadband source firstly passes through the TOF and then

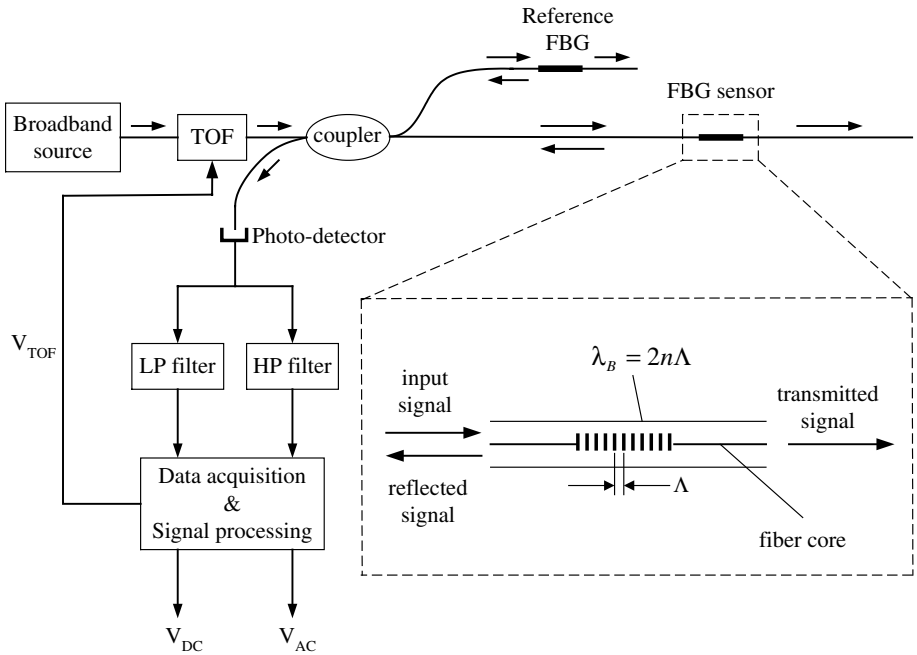


Fig. 1. A schematic of the FBG sensing system (adapted from Ho et al. [23] and Kersey et al. [24]). LP and HP stand for low pass and high pass, respectively.

split into two by the fiber coupler, one to the sensing FBG, the other to the reference FBG. Light reflected from the two FBGs are combined by the same coupler and fed into the photo-detector. The photo-detector converts optical signal to electrical signal that is further processed to give two outputs, one ($V_{DC}$) for static temperature measurement, the other ($V_{AC}$) for dynamic measurement.

As already mentioned in the last section, the FBGs are made by introducing a periodic change in the refractive index along an optic fiber (see Fig. 1). An FBG is characterized by its Bragg resonance wavelength $\lambda_B = 2n\Lambda$ [24], where $\Lambda$ is the grating pitch and $n$ the averaged fiber refractive index. When an optical fiber built with an FBG sensor is bounded on the surface of the structure along the cylinder span, the fiber and the FBG sensor will follow the surface temperature of the cylinder. Any perturbation, say due to applied temperature variation, $\theta$, on the FBG results in a variation in $\Lambda$ and $n$, and therefore a shift $\Delta\lambda_B$ in $\lambda_B$. The value of $\Delta\lambda_B$ is related to $\theta$ by $\Delta\lambda_B = K\theta$, where $K$ is a scale factor and can be determined by a calibration process.

A number of techniques have been reported for the measurement of wavelength shift $\Delta\lambda_B$ [24]. The techniques suitable for static (slow varying $\Delta\lambda_B$ or $\theta$) and dynamic (fluctuating or fast varying $\theta$) measurements are usually different. The system shown in Fig. 1 can be used for both static and fluctuating temperature measurements. The static measurement can in principle be performed by scanning the TOF and measuring the TOF control voltage $V_{TOF}$ when the output $V_{DC}$ reaches its maximum, corresponding to the center wavelength of the TOF aligned to the Bragg wavelength of the sensing FBG. In practice however the measured $V_{TOF}$ is different (not repeatable) from scan to scan even when the Bragg wavelength of the sensing FBG is kept constant. This non-repeatability problem can be overcome by using the reference FBG. The reference FBG is isolated from the environmental effect and therefore its Bragg wavelength can be regarded as constant. The actual measurement is carried out by scanning the TOF and recording the TOF control voltages $V_{TOF} = V_r$ and $V_{TOF} = V_s$, corresponding to the two maxima in $V_{DC}$ for each scan. The two maxima correspond to the center wavelength of the TOF aligned to the Bragg wavelengths of the reference and sensing FBGs, respectively. The differential voltage $V_s - V_r$ is proportional to the difference between the two Bragg wavelengths and is therefore to the applied static temperature.

The fluctuating temperature measurement is performed by the following procedure: after the aforementioned scan for static measurement is completed, the TOF control voltage $V_{TOF}$ is tuned to and held at a constant value $V_o = V_s + \Delta V_s$, corresponding to the center wavelength of the TOF aligned to a maximum slope point on the reflection spectrum of the sensing FBG. Around this operating point, the sensor response is linear and most sensitive to a small fluctuating temperature. Any temperature fluctuation applied to the sensing grating is transformed linearly into a light intensity variation that is converted into a time varying voltage ($V_{AC}$) at the photo-detector output. The value of $\Delta V_s$ is determined by the spectral characteristic of the sensing grating. By repeating the scanning-and-holding process, the static and fluctuating temperatures can be measured alternatively. The scanning-and-holding times can be adjusted and should be selected carefully to optimize the measurement performance.

## 3. Experimental details

Experiments were conducted in a suction-type wind tunnel with a 0.5 m long working section (0.35 m × 0.35 m). A brass circular cylinder of diameter $d = 19.0$ mm was vertically mounted in the mid-plane of the working section, 20 cm from the exit plane of the contraction. This resulted in a blockage of about 5.4% and an aspect ratio of 18. The cylinder vibration is negligible because of a very large structural rigidity. The cylinder was electrically heated. The Reynolds number $Re$ ($\equiv U_\infty d/\nu$, where $U_\infty$ is the free-stream velocity and $\nu$ the fluid kinematic viscosity) investigated varied from 7600 to 35 000. In the free stream, the longitudinal turbulence intensity was about 0.2%.

The experimental arrangement is shown schematically in Fig. 2. The wake fluctuating velocity $u$ was monitored by a single tungsten hot wire of 5 μm in diameter and 2.5 mm in length placed at $x/d = 2$ and $y/d = 1.5$, where $x$ and $y$ are the streamwise and lateral coordinates, respectively, whose origin is chosen at the cylinder center. The hot wire was operated at an overheat ratio of 1.8 with a constant temperature anemometer.

A groove of about 125 μm deep was made along the cylinder span to lay an optical fiber of diameter 125 μm. The fiber, flush with the cylinder surface using heat-conducting silicone, was built with an FBG sensor. The sensor, located at the mid-span of the cylinder, measured the static temperature $\overline{\theta_s}$ and fluctuating temperature $\theta_s$ on the cylinder surface. The sensor grating (built in the optical fiber) has a finite length, i.e. about 10 mm ($\approx 0.5d$) in the present investigation. The measured temperature represents an average value over this length. As the boundary layer separates from the cylinder, the vortex cell is characterized by a typical spanwise extent of 1–3$d$ [3,25]. Therefore, The temperature along the sensor grating should be statistically identical, which was considered to be the local temperature at the mid-span of the cylinder. By rotating the cylinder, the circumferential distribution of temperature was measured. Assuming a symmetrical distribution about the $x$-axis,

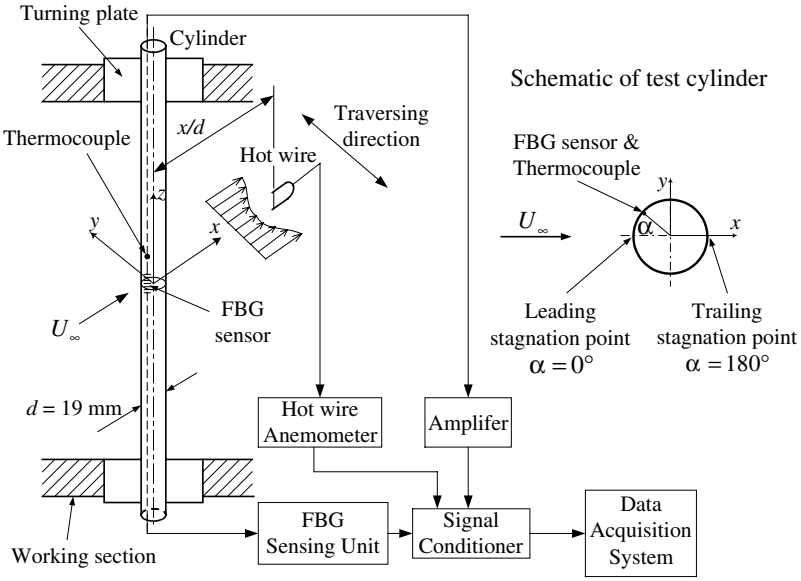


Fig. 2. Experimental arrangement.

$\overline{\theta_s}$ and $\theta_s$ were measured from $\alpha = 0°$ to 180° only, where $\alpha = 0°$ and 180° corresponds to the leading and trailing stagnation points, respectively. In order to validate the FBG sensor measurement, $\overline{\theta_s}$ was simultaneously measured using a type-*K* thermocouple of 0.3 mm diameter placed at the same $\alpha$ as the FBG sensor but 0.02 m ($\approx 1d$) away in the spanwise direction. At such small spanwise distance, say $1d$, the static surface temperature captured by the thermocouple should be the same as that by the FBG sensor [3,25].

Generally speaking, there is a difference between the surface temperature and the measured temperature [14]. Two factors may be responsible for this temperature difference. Firstly, the contact of the sensor with the investigated surface may alter the local heat flow and hence the temperature field. Secondly, the thermal contact resistance between the sensor and the investigated surface. However, the diameter of sensor grating (bare fiber) is 62.5 μm only. The sensor grating was buried using heat-conducting silicone in a groove along the brass cylinder, whose thermal conductivity is excellent. Therefore, the temperature difference and the possible thermal inhomogeneity over the cylinder surface should be negligible.

The signals $u$, $\theta_s$ and $\overline{\theta_s}$ were simultaneously measured and amplified and then digitized using a 12 bit A/D board and a personal computer at a sampling frequency of 3.5 kHz per channel. The duration of each record was 20 s. This has been verified to be sufficiently long for the root mean square (rms) value, $\theta_{s,rms}$, of $\theta_s$ to reach approximately constant, with a variation smaller than 1.0%.

## 4. Static temperature

For the purpose of comparison, the measured temperature is normalized by the overall mean surface temperature, $\Theta = (1/n)\sum_{i=1}^{n} \overline{\theta_s}(\alpha_i)$, where $\overline{\theta_s}(\alpha_i)$ represents the measured local static surface temperature and $n$ is the total number of $\overline{\theta_s}$ measured around the cylinder surface for each *Re*. Fig. 3 presents both FBG sensor and thermocouple measurements of $\overline{\theta_s}/\Theta$ at $Re = 7600$. The two techniques show a good agreement, thus providing a validation for the FBG sensor measurement.

The circumferential distribution of the heat transfer coefficient, i.e. the Nusselt number *Nu*, around the cyl-

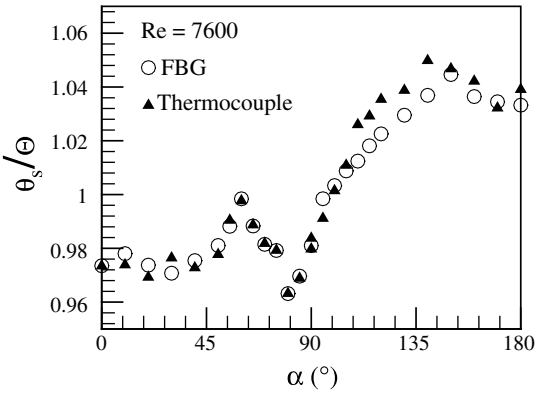


Fig. 3. Circumferential distributions of the local static surface temperature $\overline{\theta_s}/\Theta$ measured using the FBG sensor (○) and a type-*K* thermocouple (▲) ($Re = 7600$).

inder surface has been well documented for different *Re* [5,6,26]. The circumferential distribution of $\overline{\theta_s}/\Theta$ is qualitatively consistent with the reported *Nu* data [27]. Before flow separation, as $\alpha$ increases, the heat transfer is adversely affected by the growing laminar boundary layer and thus *Nu* gradually decreases. *Nu* reaches the minimum at the point of the boundary layer separation. Correspondingly, $\overline{\theta_s}/\Theta$ rises from $\alpha = 0°$ up to 60° (Fig. 3), which is likely to correspond to the minimum local *Nu* or approximately the flow separation point. Indeed, the extrapolation of Giedt's [5] measurement of *Nu* at *Re* larger than in the present investigation indicates that the minimum *Nu* occurs around $\alpha \approx 60°$ for the present *Re*. It is worthwhile pointing out that the separation point oscillates and its excursion is usually within 10°, varying from $\alpha = 75°$ to 85° for $Re = 1.06 \times 10^5$ [2]. The mean location of flow separation is dependent upon *Re* [4]. For example, Higuchi et al. [3] found that the separation point oscillated between 87° and 95° at $Re = 1.96 \times 10^5$, while Achenbach [1] reported that boundary layer separation occurred at 78° for $Re = 10^5$ and shifted to 94° for $Re = 3 \times 10^5$. Again, these experimental data may be extrapolated, suggesting the occurrence of the separation point near $\alpha \approx 60°$. There is a subsequent drop between $\alpha \approx 60°$ and 80° in $\overline{\theta_s}/\Theta$ due to a corresponding increase in *Nu*. The increased *Nu* results from the turbulent motion in the separated flow, which may perturb the laminar sublayer that is responsible to the main thermal resistance associated with the convective heat transfer [27]. For $\alpha > 80°$, $\overline{\theta_s}/\Theta$ climbs steadily probably due to the recirculation effect. Since vortex shedding would produce a strong back-flow over the rear portion of the cylinder [28], the local heat transfer coefficient increases. Consequently, $\overline{\theta_s}/\Theta$ decreases slightly near the trailing stagnation point ($\alpha = 180°$).

## 5. Fluctuating temperature

### 5.1. Time series and their spectra

Figs. 4(a)–(c) show the time histories of $\theta_s$ at $\alpha = 0°$ (upper trace) and $\alpha = 80°$ (middle trace), where the minimum $\overline{\theta_s}/\Theta$ occurs, along with the simultaneously measured $u$ (lower trace), for different *Re*. The same scale is used for the signals at different *Re* to facilitate comparison. For all *Re*, the $\theta_s$ signal at $\alpha = 80°$ exhibits a quasi-periodic fluctuation, which is also evident in the $u$ signal, apparently due to vortex shedding. In general, the maximum amplitude of $\theta_s$ grows with *Re*. The $\theta_s$ signal at $\alpha = 0°$ is quite different from that at $\alpha = 80°$. A pseudo-periodic fluctuation is also evident, but its magnitude is much smaller than at $\alpha = 80°$. Furthermore, the dominant fluctuation frequency appears higher. The dominant frequencies are better identified in the power spectra, $E_{\theta_s}$ and $E_u$ (Fig. 5), of $\theta_s$ and $u$ ($Re = 15\,200$). Here, $E_{\theta_s}$ (also $E_u$) is normalized so that $\int_0^\infty E_{\theta_s}(f)\,\mathrm{d}f = 1$. Both $E_{\theta_s}$ and $E_u$ display one major peak at $f_s^* = f_s d/U \approx 0.2$, which is consistent with the vortex shedding frequency of a single cylinder [29]. Another peak in $E_{\theta_s}$ occurs at $f^* \approx 0.4$, which is probably the second harmonic of $f_s^*$. This peak is more evident at $\alpha = 0°$, where $\theta_s$ reflects vortex shedding on both sides. The observation is consistent with Scholten and Murray's [7] report in that the time trace of the heat flux signal at the forward stagnation point fluctuated at $2f_s^*$. It is pertinent to comment that $E_{\theta_s}$ and $E_u$ display identical dominant frequencies at say $f_s^*$. This is confirmed for all the *Re* investigated, suggesting that the FBG sensor has a small thermal inertia and its dynamic response is adequate to resolve the fluctuating temperature on the cylinder surface.

The test cylinder, fix-supported at both ends, may vibrate due to vortex excitation forces, which produces a structural dynamic strain [30]. The strain may reflect on the optic fiber, leading to a shift $\Delta\lambda_B$ in $\lambda_B$ [21,22]. Consequently, the measured fluctuating temperature signal might be disturbed. It is therefore important to ensure a negligible contamination in the present investigation. A test was thus conducted at conditions identical to those described for the fluctuating temperature measurements in Section 3, except the cylinder was unheated. Fig. 6 presents the signal (the same scale as that in Fig. 4) recorded in the test by the FBG sensor at $Re = 15\,200$ and $\alpha = 80°$, along with the velocity signal $u$. Evidently, the signal is largely due to the structural vibration and background noise. Its amplitude is greatly reduced, compared with that at the same *Re* and $\alpha$ when the cylinder was heated (Fig. 4b). In fact, the maximum ratio of $\theta_{s,rms}$ with the cylinder heated to that without heating is about 6 (near $\alpha = 80°$), while the minimum is about 2. This is a good indication of the signal-to-noise ratio range. Furthermore, the corresponding $E_{\theta_s}$ (not shown) does not show any peak at $f_s^* \approx 0.2$. These results point to a negligible effect of the structural vibration on the present temperature measurement.

### 5.2. Closely correlated $\theta_s$ and $u$

The spectral coherence $\mathrm{Coh}_{\theta_s u}$ ($\equiv (\mathrm{Co}_{\theta_s u}^2 + Q_{\theta_s u}^2)/E_{\theta_s}E_u$, where $\mathrm{Co}_{\theta_s u}$ and $Q_{\theta_s u}$ are the co-spectrum and quadrature spectrum of $\theta_s$ and $u$, respectively) provides a measure of the degree of correlation between the Fourier components of $\theta_s$ and $u$. $\mathrm{Coh}_{\theta_s u}$ (Fig. 7) between $\theta_s$ ($\alpha = 80°$) and $u$ reaches 0.9 at $f_s^* \approx 0.2$, indicating a high level of correlation. This observation is consistent with the fact that the fluctuating temperature on the cylinder surface is closely linked to the vortex formation and shedding. The highly correlated $\theta_s$ and $u$ lend further credence to the present measurement technique.

Note that the dynamic response of the FBG sensor *per se* could reach over 20 kHz [23]. However, the

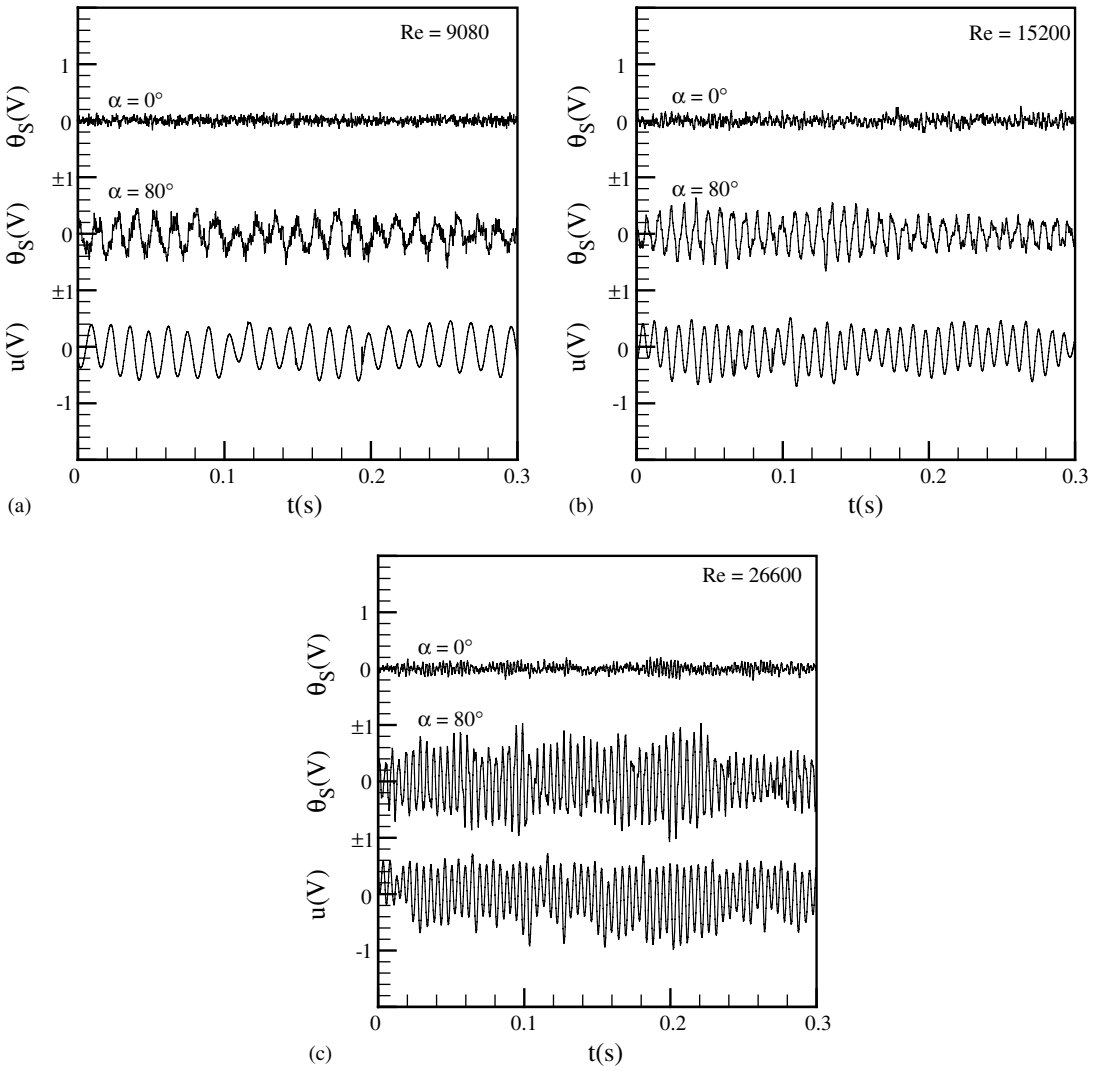


Fig. 4. Time histories of $u$ (the hot wire was located at $x/d = 2$ and $y/d = 1.5$) and $\theta_s$ at $\alpha = 0°$ and 80° (time $t = 0$ is arbitrary). (a) $Re = 9080$; (b) $Re = 15200$; (c) $Re = 26600$.

dynamic response may be adversely affected by the thermal inertia of heat-conducting silicone between the cylinder surface and grating. Because this silicon layer is extremely thin, its effect on the dynamic response of the sensor should be minimum, as corroborated by the excellent correlation between $\theta_s$ and $u$ (Fig. 7).

The spectral phase shift $\Phi_{\theta_s u}$ ($\equiv \tan^{-1} Q_{\theta_s u}/\mathrm{Co}_{\theta_s u}$) between $\theta_s$ and $u$ at $f_s^*$ (Fig. 8) tends to be anti-phased, approaching $\pi$, irrespective of the $\alpha$ value ($Re = 15200$). The corresponding $\mathrm{Co}_{\theta_s u}$ exhibits a negative extremum at $f_s^*$, as illustrated in Fig. 9. The location of the hot wire was unchanged throughout the experiments. The observation is reasonable. When the boundary layer separates from the cylinder surface, the streamwise velocity measured by the hot wire at $x/d = 2$ and $y/d = 1.5$ should be increased, giving rise to a positive $u$. Meanwhile, heat is removed from the cylinder surface, resulting in a negative $\theta_s$.

### 5.3. Probability density function

The probability density function (PDF), $P_{\theta_s}$, of $\theta_s$ (Fig. 10) at $\alpha = 80°$ ($Re = 15200$) is quite symmetrical about $\theta_s/\theta_{s,\mathrm{rms}} = 0$ and appears to follow the normal distribution. The maximum magnitude of $\theta_s$ approximately triples $\theta_{s,\mathrm{rms}}$. This observation is essentially in consistence with Boulos and Pei's [26] investigation on the heat transfer from a circular cylinder in a turbulent

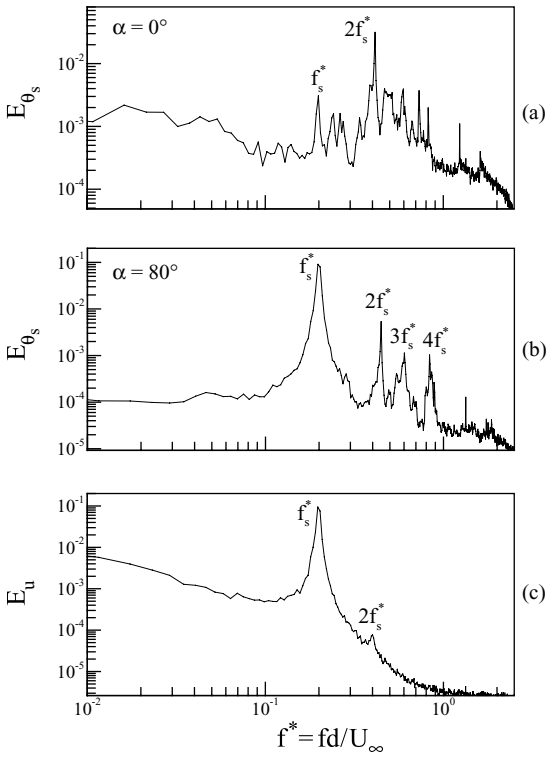


Fig. 5. Power spectrum $E_{\theta_s}$ of the fluctuating surface temperature $\theta_s$ and $E_u$ of the streamwise fluctuating velocity $u$ in the wake. $Re = 15200$. (a) $E_{\theta_s}$ at $\alpha = 0°$; (b) $E_{\theta_s}$ at $\alpha = 80°$; (c) $E_u$. The hot wire was located at $x/d = 2$ and $y/d = 1.5$.

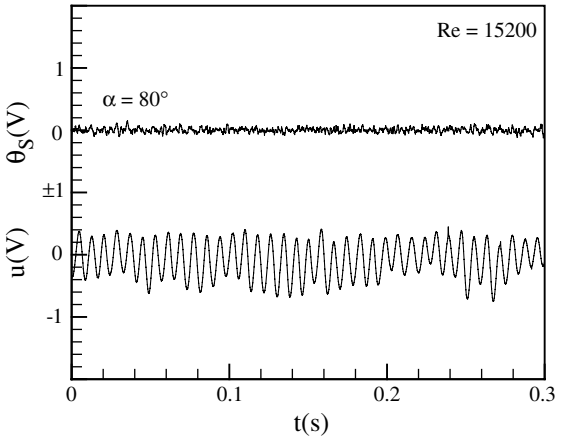


Fig. 6. Time histories of the streamwise fluctuating velocity $u$ (the hot wire was located at $x/d = 2$ and $y/d = 1.5$) and $\theta_s$ at $Re = 15200$ and $\alpha = 80°$. The cylinder was unheated.

air flow at $Re = 3000$–$9000$. Their results indicated that the PDF of the measured heat transfer rate is normal

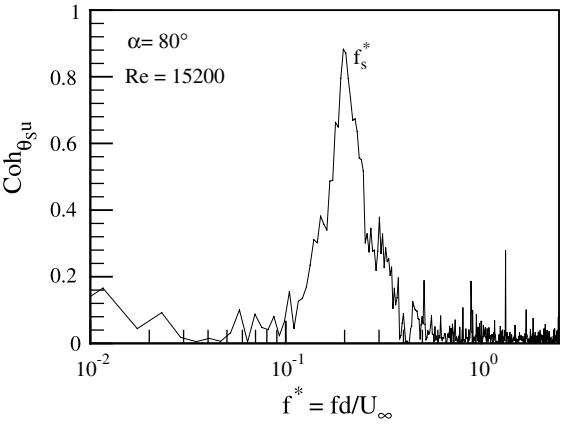


Fig. 7. Spectral coherences $\mathrm{Coh}_{\theta_s u}$ between the fluctuating surface temperature $\theta_s$ and the streamwise fluctuating velocity $u$ at $\alpha = 80°$ and $Re = 15200$. The hot wire was located at $x/d = 2$ and $y/d = 1.5$.

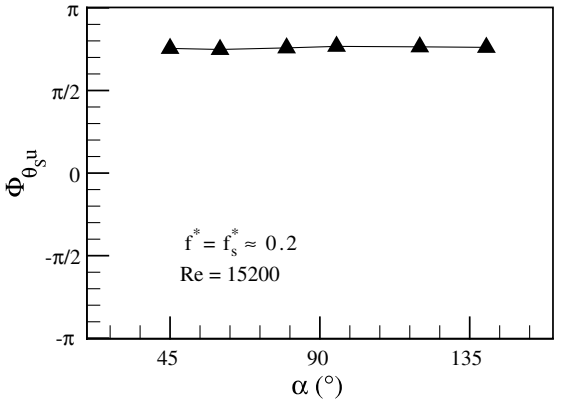


Fig. 8. Spectral phase angle $\Phi_{\theta_s u}$ at various $\alpha$ between the fluctuating surface temperature $\theta_s$ and the streamwise fluctuating velocity $u$ ($Re = 15200$). The hot wire was located at $x/d = 2$ and $y/d = 1.5$.

around the flow separation point (e.g. at $\alpha = 80°$–$90°$) under both constant wall temperature and constant heat flux conditions.

### 5.4. Circumferential distribution of $\theta_{s,rms}$

The circumferential distribution of $\theta_{s,rms}$ for $Re = 9080$, 15200 and 26600 is given in Fig. 11. The $\theta_{s,rms}/\Theta$ value displays a maximum near $\alpha \approx 80°$ for the present range of $Re$ (Fig. 11). This location is coincident with the minimum static temperature (Fig. 3). Both observations may be attributed to the turbulent eddy motion after flow separation. On the other hand, the

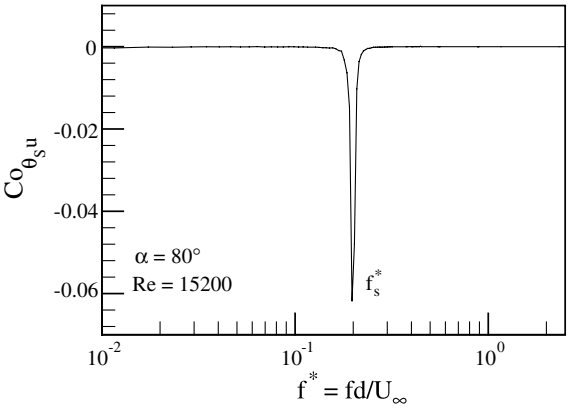


Fig. 9. Co-spectrum $Co_{\theta_s u}$ between the fluctuating surface temperature $\theta_s$ and the streamwise fluctuating velocity $u$ at $\alpha = 80°$ and $Re = 15200$. The hot wire was located at $x/d = 2$ and $y/d = 1.5$.

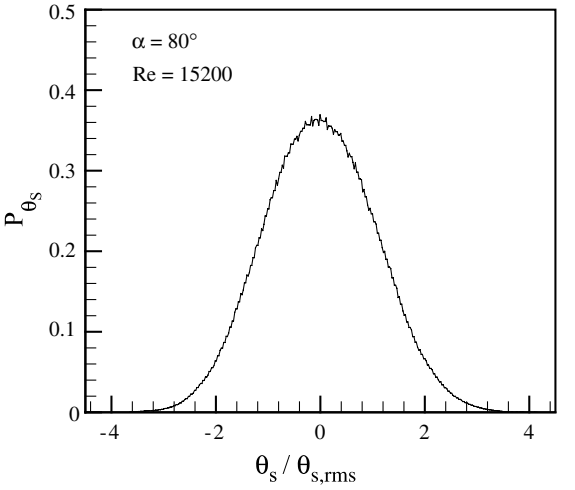


Fig. 10. The PDF $P_{\theta_s}$ of the fluctuating surface temperature $\theta_s$ measured using the FBG sensor. $Re = 15200$, $\alpha = 80°$.

minimum $\theta_{s,rms}/\Theta$ occurs at the leading and trailing stagnation points. The present observation conforms to Scholten and Murray's [7] heat flux measurement, which indicated a great fluctuation in the heat flux on the cylinder surface at $\alpha = 85°$, compared with that at $\alpha = 0°$ ($Re = 21580$).

The maximum value of $\theta_{s,rms}/\Theta$ (Fig. 12) increases for larger $Re$. Krall and Eckert [6] proposed that the boundary layer around a circular cylinder subjected to a uniform cross-flow became rapidly thinner as $Re$ increases. This implies that the cylinder surface temperature is more prone to the vortex formation and shedding perturbation, fluctuating more with increasing $Re$ (Figs. 11 and 12), especially near the flow separation region.

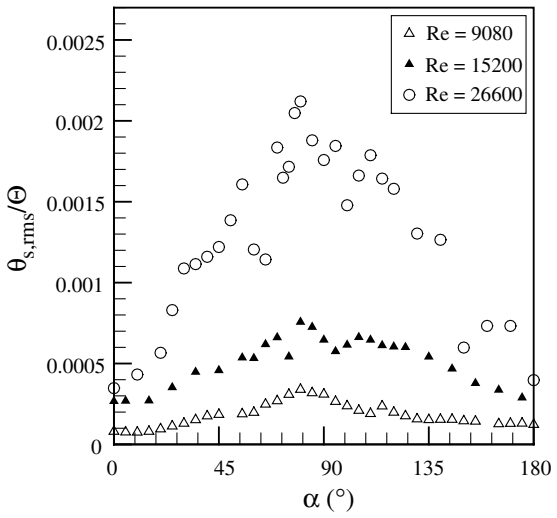


Fig. 11. Circumferential distribution of the rms value $\theta_{s,rms}/\Theta$ of the fluctuating surface temperature $\theta_s$. (△) $Re = 9080$; (▲) $Re = 15200$; (○) $Re = 26600$.

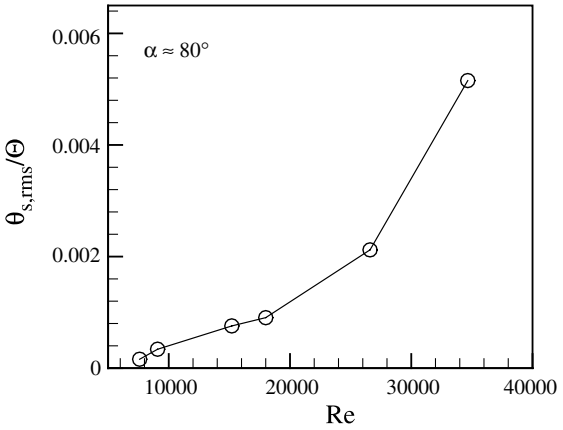


Fig. 12. Influence of $Re$ on the maximum rms value, $\theta_{s,rms}/\Theta$, of the fluctuating surface temperature $\theta_s$ near $\alpha \approx 80°$.

## 6. Conclusions

Attempt has been made to use the FBG sensor to measure simultaneously static and fluctuating surface temperatures on a heated circular cylinder in a cross-flow. The investigation leads to the following conclusions:

1. The local static surface temperature $\overline{\theta_s}/\Theta$ measured using the FBG sensor is in good agreement with that simultaneously obtained by a $K$-type thermocouple. Furthermore, the circumferential distribution of $\overline{\theta_s}/\Theta$ is qualitatively consistent with the reported $Nu$ data. At $Re = 7600$, for example, a maximum $\overline{\theta_s}/\Theta$ occurs at

$\alpha \approx 60°$, corresponding to the minimum heat transfer coefficient *Nu* and probably to the flow separation point. As $\alpha$ increases from 60° to 80°, $\overline{\theta_s}/\Theta$ drops rapidly, reaching the minimum at $\alpha \approx 80°$; accordingly, there is a quick climb in *Nu*. The observation is probably due to the turbulent eddy motion after flow separation, which is supported by a prominent peak in the rms value $\theta_{s,rms}$ of $\theta_s$ near $\alpha \approx 80°$. For further increase in $\alpha$, $\overline{\theta_s}/\Theta$ increases due to a decrease in *Nu*. The results suggest that the FBG sensor can provide reliable measurements for the static temperature on the cylinder surface.

2. The dynamic response of the FBG sensor is excellent. The fluctuating temperature $\theta_s$ is closely correlated to the hot-wire measurement. The power spectrum $E_{\theta_s}$ exhibits a prominent peak at the vortex shedding frequency $f_s^* \approx 0.2$, as identified in $E_u$. The $\theta_s$- and *u*-signals tend to be anti-phased at $f_s^*$, their spectral coherence reaching 0.9 conforming to the underlying physical relationship between temperature fluctuation and velocity fluctuation. These results indicate that the FBG sensor is excellent in resolving the fluctuating surface temperature of a cylinder in a cross-flow.

In view of the uniqueness in many aspects and being at an affordable cost, it is expected that the FBG sensor may have an excellent prospect in the measurements of both static and fluctuating temperatures.

## Acknowledgements

The authors wish to acknowledge support by the Central Research Grant of The Hong Kong Polytechnic University through Grants G-T408, G-YD21 and G-T444, and by the Hong Kong SAR government through a CERG grant PolyU5105/99E.

## References

[1] E. Achenbach, Distribution of local pressure and skin friction around a circular cylinder in cross-flow up to $Re = 5 \times 10^6$, J. Fluid Mech. 34 (4) (1968) 625–639.
[2] H.A. Dwyer, W.J. Mccroskey, Oscillating flow over a cylinder at large Reynolds number, J. Fluid Mech. 61 (4) (1973) 753–767.
[3] H. Higuchi, H.J. Kim, C. Farell, On flow separation and reattachment around a circular cylinder at critical Reynolds numbers, J. Fluid Mech. 200 (1989) 149–171.
[4] S.S. Chen, Flow-Induced Vibration of Circular Cylindrical Structures, Hemisphere Publishing Corporation, Washington, 1987.
[5] W.H. Giedt, Investigation of variation of point unit heat-transfer coefficient around a cylinder normal to an air stream, Trans. ASME (1949) 375–381.
[6] K.M. Krall, E.R.G. Eckert, Local heat transfer around a cylinder at low Reynolds number, J. Heat Transfer 95 (1973) 273–275.
[7] J.W. Scholten, D.B. Murray, Unsteady heat transfer and velocity of a cylinder in cross flow: part 1. Low freestream turbulence, Int. J. Heat Mass Transfer 41 (10) (1998) 1139–1148.
[8] H.C. Perking Jr., G. Leppert, Local heat-transfer coefficients on a uniformly heated cylinder, Int. J. Heat Mass Transfer 7 (1964) 143–158.
[9] A. Zukauskas, J. Ziugzda, Heat Transfer of a Cylinder in Crossflow (E. Bagdonaite, Trans.; edited by G.F. Hewitt), Hemisphere Pub, Washington, 1985.
[10] M.I. Boulos, D.C.T. Pei, Heat and mass transfer from cylinders to a turbulent fluid stream—A critical review, Can. J. Chem. Eng. 51 (12) (1973) 673–679.
[11] J.W. Valvano, Temperature measurements, Adv. Heat Transfer 22 (1992) 359–436.
[12] A.S. Morris, Principles of Measurement and Instrumentation, second ed., Redwood Books Ltd., Trowbridge, Wiltshire, Great Britain, 1993.
[13] R.A. Antonia, Y. Zhou, M. Matsumara, Spectral characteristics of momentum and heat transfer in the turbulent wake of a circular cylinder, Exp. Thermal Fluid Sci. 6 (1992) 371–375.
[14] L. Michalski, K. Eckersdorf, J. McGhee, Temperature Measurement, John Wiley & Sons Ltd., Baffins Lane, Chichester, England, 1991.
[15] L. Marton, C. Marton, in: Fluid Dynamics, Part B, Methods of Experimental Physics, vol. 18, Academic Press, Inc. (London) Ltd., 1981.
[16] M. Gottlieb, G.B. Brandt, Measurement of temperature with optical fibers, in: Fibre Optic Conference, Chicago, 1979, pp. 236–242.
[17] C. Sandberg, L. Haile, Fiber optic application in pipes and pipelines, IEEE Trans. Ind. Appl. IA 23 (6) (1987) 1061.
[18] K.T.V. Grattan, The use of fibre optic techniques for temperature measurement, Meas. Control 20 (6) (1987) 32–39.
[19] K.O. Hill, Y. Fujii, D.C. Johnson, B.S. Kawasaki, Photosensitivity in optical fiber waveguides: Application to reflection filter fabrication, Appl. Phys. Lett. 32 (10) (1978) 647–649.
[20] W.W. Morey, G. Meltz, W.H. Glenn, Bragg-grating temperature and strain sensors, The Sixth Optical Fibre Sensor Conference, Paris, Springer Proc. 44 (1989) 526–531.
[21] Y. Zhou, R.M.C. So, W. Jin, H.G. Xu, P.K.C. Chan, Dynamic strain measurements of a circular cylinder in a cross flow using a fibre Bragg grating sensor, Exp. Fluid 27 (1999) 359–367.
[22] W. Jin, Y. Zhou, P.K.C. Chan, H.G. Xu, A fibre-optic grating sensor for the study of flow-induced vibrations, Sens. Actuators 79 (2000) 36–45.
[23] H.L. Ho, W. Jin, C.C. Chan, Y. Zhou, X.W. Wang, A fiber Bragg grating sensor for static and dynamic measurands, Sens. Actuators A 96 (2002) 21–24.
[24] A.D. Kersey, M.A. Davis, H.J. Patrick, M. LeBlanc, K.P. Koo, C.G. Askins, M.A. Putnam, E.J. Friebele, Fiber grating sensors, J. Lightwave Technol. 15 (1997) 1442–1462.
[25] R. King, A review of vortex shedding research and its application, Ocean Eng. 4 (1977) 141–171.

[26] M.I. Boulos, D.C.T. Pei, Dynamics of heat transfer from cylinders in a turbulent air stream, Int. J. Heat Mass Transfer 17 (1974) 767–783.
[27] J.P. Holman, Heat Transfer, eighth ed., McGraw-Hill Companies, New York, 1997, pp. 248–255 and 303.
[28] S. Goldstein, Modern Developments in Fluid Mechanics: An Account of Theory and Experiment Relating to Boundary Layers, Turbulent Motion and Wakes, Dover Publications, Inc., New York, 1965.
[29] H. Schlichting, Boundary-Layer Theory, McGraw-Hill, New York, 1979.
[30] Y. Zhou, Z.J. Wang, R.M.C. So, S.J. Xu, W. Jin, Free vibrations of two side-by-side cylinders in a cross flow, J. Fluid Mech. 443 (2001) 197–229.